ARMY RESEARCH LABORATORY

Computational Fluid Dynamic (CFD) Analysis of a Generic Missile With Grid Fins

by James DeSpirito, Harris L. Edge, Paul Weinacht,
Jubaraj Sahu, and Surya Dinavahi

ARL-TR-2318   September 2000

20001018 006

Abstract

This report presents the results of a study demonstrating an approach for using viscous computational fluid dynamic simulations to calculate the flow field and aerodynamic coefficients for a missile with grid fins. A grid fin is an unconventional lifting and control surface that consists of an outer frame supporting an inner grid of intersecting planar surfaces of small chord. The calculations were made at a Mach number of 2.5 and several angles of attack for a missile without fins, with planar fins, and with grid fins. The results were validated by comparing the computed aerodynamic coefficients for the missile and individual grid fins against wind tunnel measurement data. Very good agreement with the measured data was observed for all configurations investigated. For the grid fin case, the aerodynamic coefficients were within 2.8–6.5% of the wind tunnel data. The normal force coefficients on the individual grid fins were within 11% of the test data. The simulations were also successful in calculating the flow structure around the fin in the separated-flow region at the higher angles of attack. This was evident in the successful calculation of the nonlinear behavior for that fin, which showed negative normal force at the higher angles of attack. The effective angle of attack is negative on either part of or all of the top grid fin for the higher angles of attack.

Acknowledgments

INTENTIONALLY LEFT BLANK.

Table of Contents

INTENTIONALLY LEFT BLANK.

List of Figures

List of Tables

INTENTIONALLY LEFT BLANK.

1. Introduction

The U.S. Army Research Laboratory (ARL) is using computational fluid dynamics (CFD) to investigate the aerodynamic characteristics and flow field structure of grid fins, also known as lattice controls. A grid fin is an unconventional lifting and control surface that consists of an outer frame supporting an inner grid of intersecting planar surfaces of small chord. Grid fins have been employed on some Soviet missiles, but have not been included on any missile systems in the West (Simpson and Sadler 1998). Interest in grid fins is primarily geared toward their potential use on highly maneuverable munitions due to their advantages over conventional planar controls at high angles of attack and high Mach number.

The aerodynamics of grid fins have been investigated since 1985 by the U.S Army Aviation and Missile Research and Development Center (AMRDEC), Huntsville, Alabama (Washington and Miller 1998, Miller and Washington 1994, and Washington and Miller 1993). These investigations indicated that grid fins have some advantages over conventional, planar fins. One advantage is the ability to maintain lift at higher angles of attack since grid fins do not have the same stall characteristics of planar fins. Another is the very small hinge moment, which can reduce the size of control actuator systems. Since curvature of the grid fins had little effect on their performance, folding down the fins onto the missile body is a storage design advantage. The main disadvantage was higher drag than that of planar fins, although techniques for minimizing drag by altering the grid fin frame cross-section shape were demonstrated (Miller and Washington 1994). These studies also showed that grid fins experience a loss in control effectiveness in the transonic regime due to flow choking in the individual cells.

The Defence Evaluation and Research Agency (DERA), United Kingdom, has performed wind tunnel tests on grid fins and compared their aerodynamic characteristics to conventional planar fins (Simpson and Sadler 1998, and Simpson 1997). These studies confirmed some of the previous results and showed improved yaw stability due to the ability of the grid fins to generate

side force. The results also showed that the vertical fins contribute about 30% of the static longitudinal stability when oriented in the cruciform (+) configuration.

Aeroballistic range flight tests have recently been conducted at the U.S. Air Force Research Laboratory Aeroballistic Research Facility (ARF), Eglin Air Force Base, Florida (Abate et al. 2000, and Abate et al. 1999). These were the first reported subscale free-flight tests of a missile configuration with grid fins. In addition to providing the raw data to derive the aerodynamic coefficients for the grid fin models, shadowgraphs of the models in flight at Mach numbers between 0.39 and 1.65 showed an interesting shock structure in and around the fins.

There have also been theoretical and numerical methods used to estimate the lift characteristics of grid fins. Methods have been developed for the subsonic (vortex lattice theory), transonic (empirical methods), and supersonic (Evvard's theory) regimes (Kretzschmar and Burkhalter 1998, Burkhalter 1996, Tong et al. 1996, Burkhalter and Frank 1996, and Burkhalter et al. 1995). Empirical extensions were used to gain data for missiles at large angles of attack. If body upwash terms are included, these methods provide adequate aerodynamic characteristics of grid fins for preliminary design purposes in the subsonic and supersonic regimes.

The first reported CFD calculations made on grid fins were sponsored by the Defence Research Establishment, Valcartier (DREV), Canada (Chen et al. 2000, Khalid et al. 1998, Sun and Khalid 1998, and Lesage 1998). These studies only included inviscid (Euler) simulations, mainly due to a lack of high performance computing resources. The authors concluded that the inviscid CFD calculations provided a reliable means of studying the flows past missiles with grid fins. Comparisons with data from Washington and Miller (1993) showed reasonable agreement for the fin normal force. The Euler calculations for the grid fins compared better with the measured data than those for the planar fins. The authors attributed this to the shorter surfaces of the grid fins in the axial direction, compared to planar fins (Sun and Khalid 1998). The results of the viscous calculations from the present study help to explain this effect.

2

This report presents the results of the first viscous CFD calculations made involving a missile with grid fins. The results are validated by comparing them against wind tunnel data provided by DERA (Simpson 1997). Simulations of the missile body alone and with planar fins were also performed as part of the validation process.

2. Numerical Approach

The investigation involved using CFD to determine the flow field and aerodynamic coefficients on a 13-cal., four-finned, generic missile shape (Figure 1). The missile has a 3-cal. tangent ogive, and the fin pitch axis is located 1.5 diameters before the aft end of the missile. The analysis proceeded in three steps. The first involved the missile without fins, case B1A (Figure 1, top); the second was with the missile with planar fins, case B1AC2R (Figure 1, middle); and the third was the missile with a set of grid fins, case B1AL2R (Figure 1, bottom). The configurations were labeled according to the designations used at DERA (Simpson 1997). The span and chord of the planar fin was 1.0 cal. The span of the grid fin was 1.1 cal. and the chord was 0.17 cal. All analyses were performed at a Mach number of 2.5 and at a minimum of three angles of attack (α): 0°, 10°, and 20°. The simulations of the missile were made in the cruciform (+) configuration, and symmetry (x-z plane) was used so that only a half-plane was modeled.

Steady-state calculations were made to compute the flow field for the three cases using the commercial CFD code, FLUENT Version 5.1. The implicit, compressible (coupled), unstructured-grid solver was used. The three-dimensional, time-dependent, Reynolds-averaged Navier-Stokes (RANS) equations are solved using the finite volume method:

$$\frac{\partial}{\partial t}\int_V \mathbf{W}dV + \oint [\mathbf{F} - \mathbf{G}] \, dA = \int_V \mathbf{H}dV , \qquad (1)$$

where $\mathbf{W}$ is the vector of conservative variables, $\mathbf{F}$ is the inviscid flux vector, $\mathbf{G}$ is the viscous flux vector, $\mathbf{H}$ is the vector of source terms, V is the cell volume, and A is the surface area of the

3
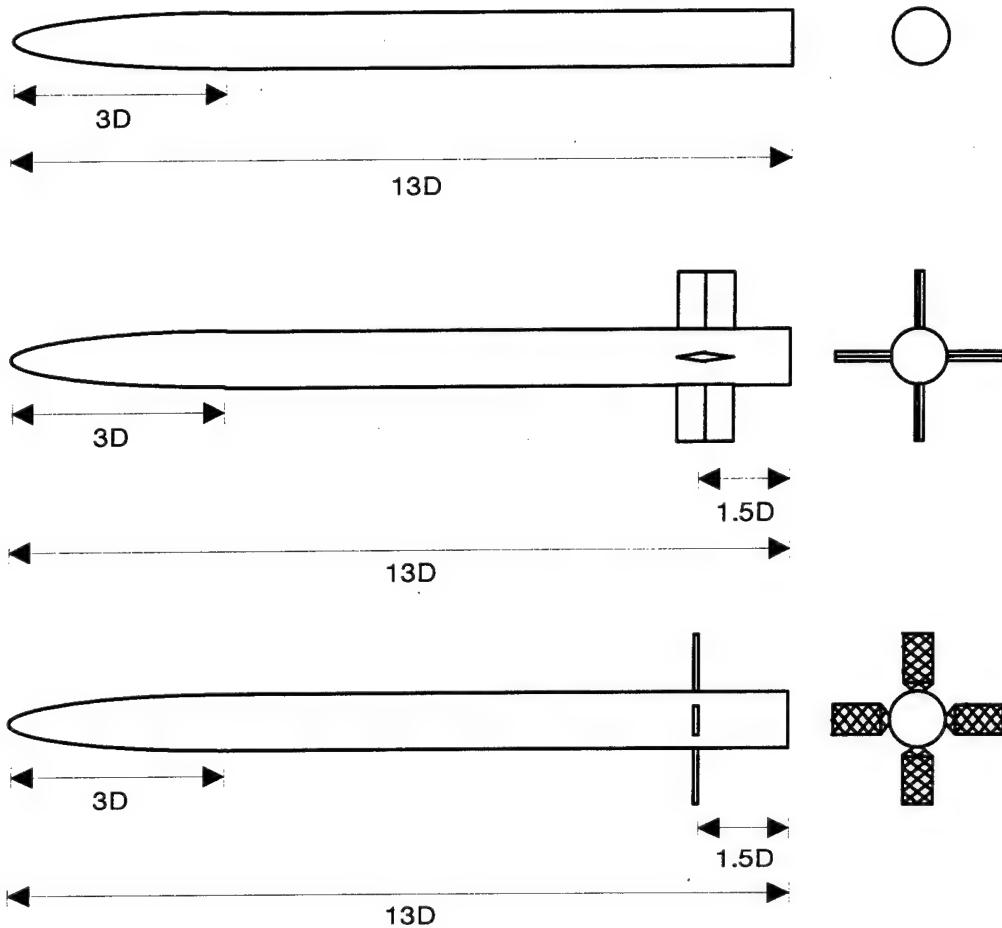
Figure 1. Basic Missile Shape With No Fins (B1A, Top), Planar Fins (B1AC2R, Middle), and Grid Fins (B1AL2R, Bottom).

cell face. The Spalart-Allmaras, one-equation turbulence model (Spalart and Allmaras 1992) was used for these calculations. In FLUENT, the original version of the Spalart-Allmaras model is modified to allow the use of wall functions when the mesh resolution is not sufficiently fine to resolve the viscous-affected, near-wall region of the boundary layer (Fluent 1998). This capability was used in generating the mesh so that the computational requirements were reduced as much as possible. Second-order discretization was used for the flow variables and the turbulent viscosity equation.

4

The geometry and unstructured meshes for the three configurations were generated using the preprocessor, GAMBIT, supplied in the FLUENT software suite. In generating the meshes, boundary layer mesh spacing was used near the missile body and fin surfaces. Advantage was taken of the wall function option of the solver in FLUENT, and the first point off the surface (cell center) was about 0.002 cal. All mesh stretching was kept below a ratio of 1.2. Hexahedral cells were used, except for a small region located ahead of and partly over the first 0.1 cal. of the nose of the missile (1% of the total length). The latter region was made up of tetrahedrons and pyramid transition elements. Figure 2 shows the mesh on the symmetry plane for the B1A case. The triangular surface mesh can be observed at the upstream end. The tetrahedral mesh was made to cover a small part of the missile nose only to allow a transition between the two types of meshes near the nose. Therefore, a true boundary layer-type mesh was not covering the first 1% of the missile body, but this had no observable effect on the results. The B1A mesh in Figure 2 was meshed as six separate volumes–one in the freestream region, two over the first 10 cal. of the missile, and two over the last 3 cal. This methodology was used so that the mesh in the first two regions could be used regardless of the fin type. The meshes between volumes were conformal, or exactly matching at the boundary surface. The total number of cells in this case was about 670,400.

The mesh on the symmetry plane for the planar fin case is shown in Figure 3. The mesh was modified slightly so that only one volume covered the first 10 cal. of the missile. The tail region, shown in Figure 4, consisted of seven volumes located ahead of, behind, and between the fins and off the fin tips. The total number of cells for this case was about 1.2 M, and again the mesh was totally conformal.

The geometry for the grid fin case is shown in Figure 5. The solid modeling capabilities of GAMBIT simplified the generation of the grid fin geometry. The mesh on the symmetry plane is shown in Figure 6. The mesh for the freestream region and the first 10 cal. of the missile body was similar to that for the planar fin case, Figure 3. Due to the complexity of the mesh in the region around the grid fins, and to minimize the total mesh size, a nonconformal mesh interface
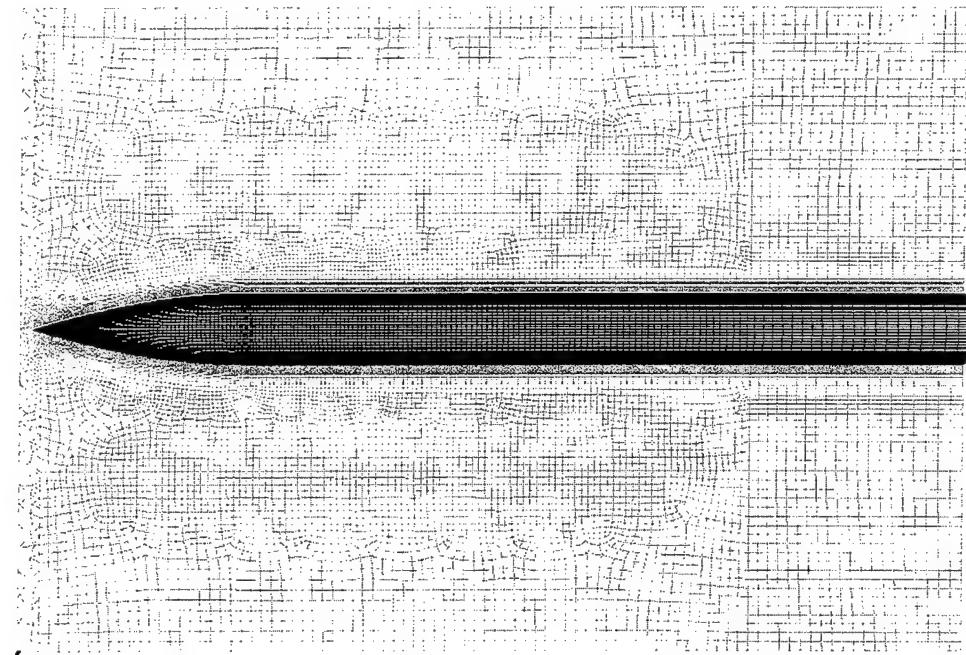
Figure 2. Unstructured Mesh for Basic Missile Shape Without Fins.
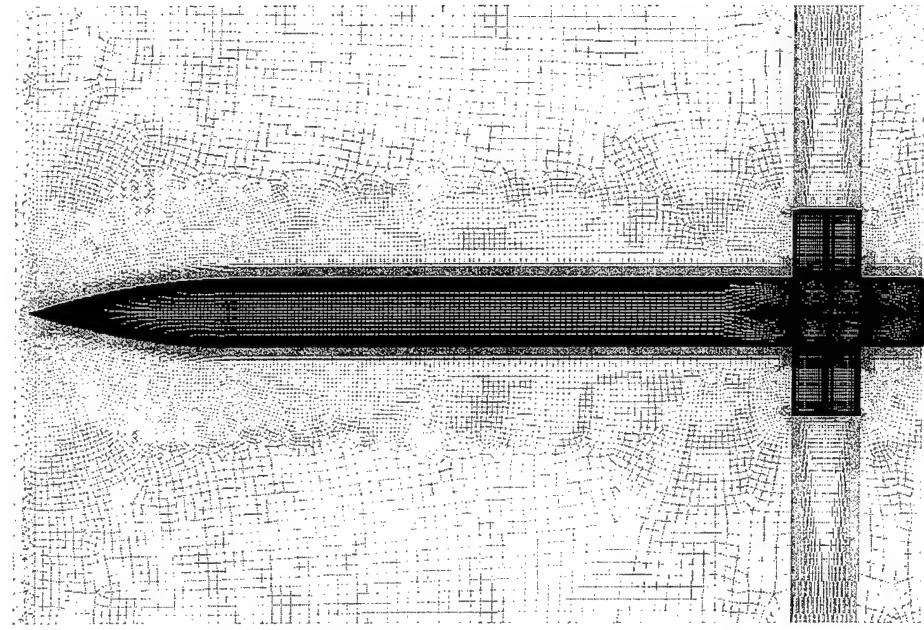
Figure 3. Unstructured Mesh for Basic Missile Shape With Planar Fins.
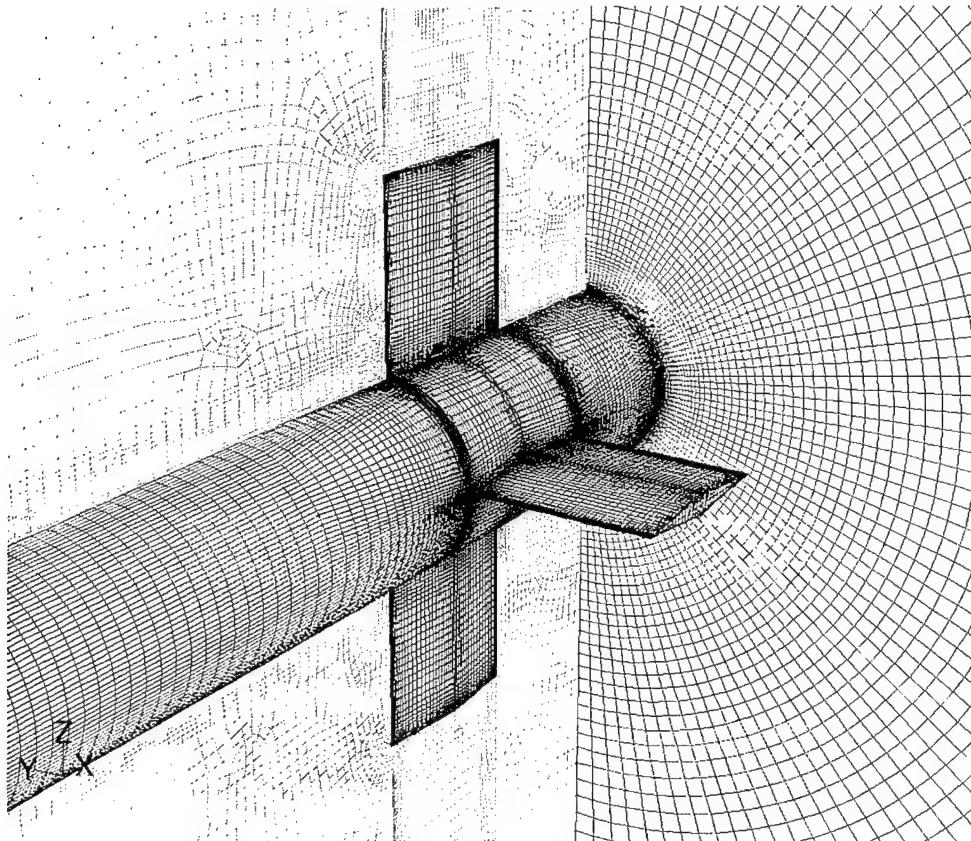
Figure 4. Unstructured Mesh in Tail Region of Planar Fin Case.

was used at the interface at 10 cal. With this type of interface, which is used in FLUENT to handle sliding meshes, the flow variables are averaged to determine the value at the interface. The total number of cells in this mesh was about 3.2 M, with 2.5 M in the fin region (10–13 cal.). The mesh in the fin region is shown in Figure 7. The fins, interior cells, and the thin region circumferentially between the fins were meshed first. The surface mesh was then projected axially forward and rearward with smoothing. A close-up of the surface mesh on the grid fin cells is shown in Figure 8. There were one or two cells across the front and rear of the grid fin web and frame surface. However, this dimension is the same order of magnitude as the first cell spacing off the surface (0.002 cal.).

The base flow was not simulated in these calculations, so the mesh stopped at the end of the missile. An outflow boundary condition was used downstream, a pressure inflow (free-stream

Z
Y—X

Figure 5. Geometry for Grid Fin Case (B1AL2R).
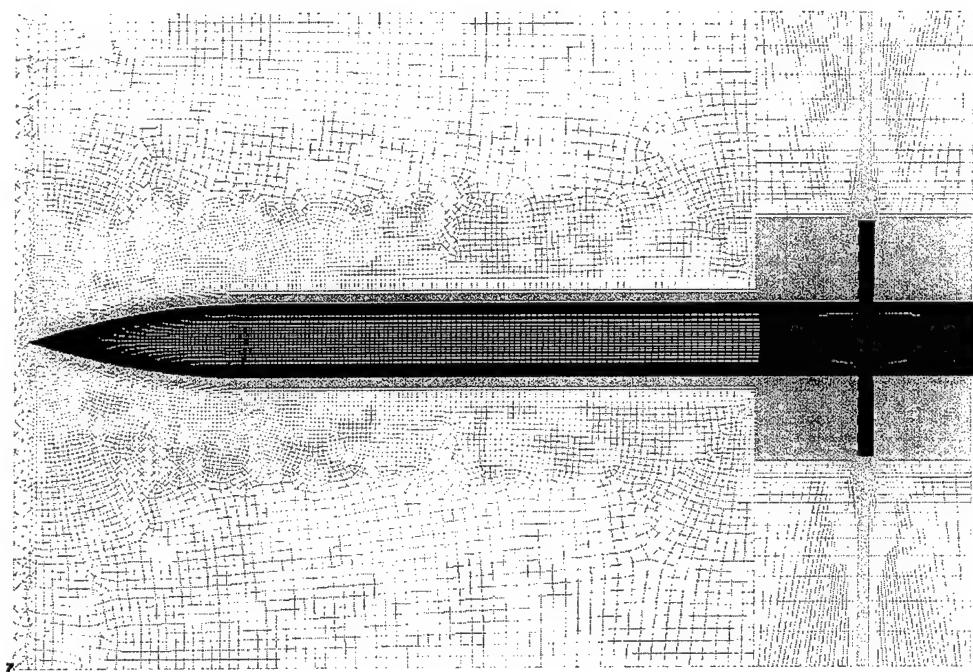
**Figure 6. Unstructured Mesh for Basic Missile Shape With Grid Fins.**
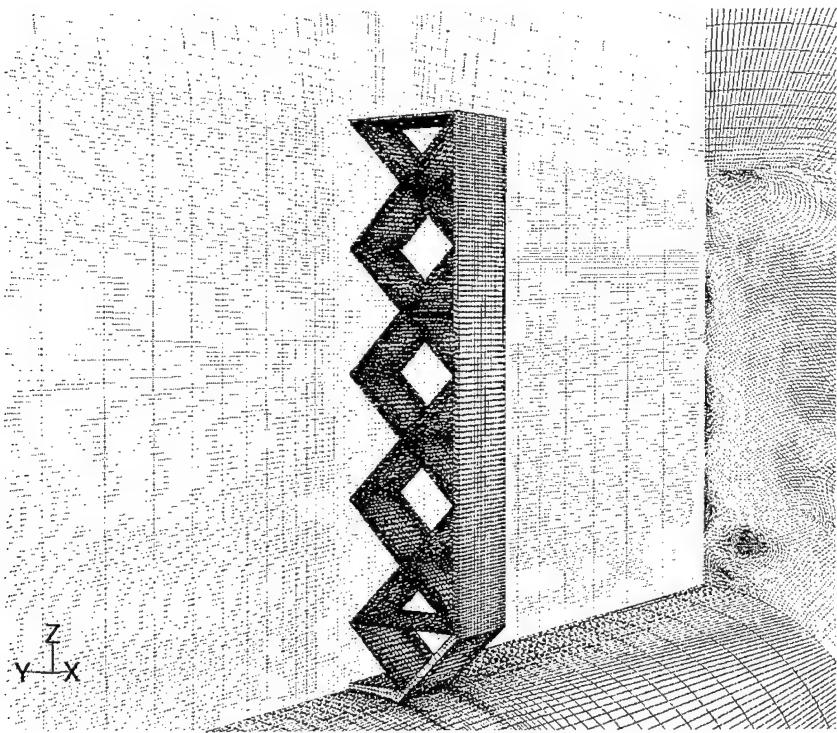
Figure 7. Unstructured Mesh in Tail Region of Grid Fin Case.
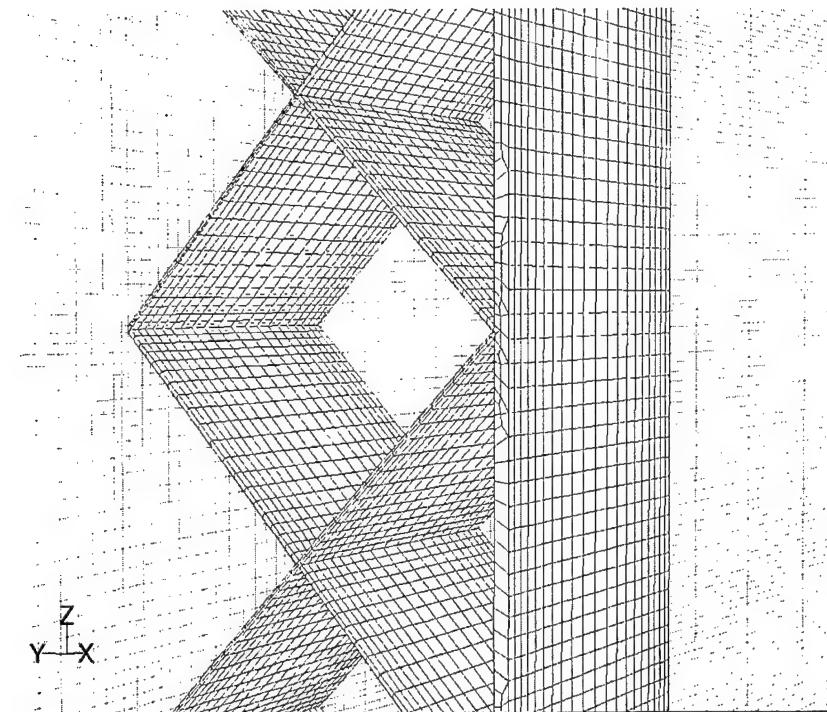
Figure 8. Surface Mesh on Grid Fin Cells.

9

conditions) boundary condition was used upstream, and a far-field pressure (nonreflecting) boundary condition was used for the outer boundary. A nonslip wall boundary condition was used for all solid surfaces. The y^+ value was about 40–60 along the missile body, which is optimal for wall functions. The maximum value was about 150 along the ogive, and between 100 and 140 on the grid fin surfaces. The Reynolds number was 13.1 x 10^6 m^{-1} (4.0 x 10^6 ft^{-1}), or 1.2 x 10^6 for this model. The freestream temperature and pressure were 137 K and 8325 Pa, respectively.

The no fin and planar fin cases were also run with a structured-mesh, implicit, finite difference code ZNSFLOW, which solved the thin-layer RANS equations. A complete description of this code can be found in the report by Edge et al. (2000). The aerodynamic coefficients calculated with this code using the Baldwin-Lomax turbulence model are presented in the next section along with those calculated with FLUENT. Since ZNSFLOW does not use wall functions in the turbulence models, the first grid point off the solid surfaces was about 5 x 10^{-6} cal., giving a y^+ value of approximately one.

The grid fin simulations were originally to be made using ZNSFLOW and a chimera overset grid (Steger et al. 1983). This is a viable approach, but the FLUENT code was chosen for the grid fin calculations because the geometry was already created using the GAMBIT preprocessor, and we believed that mesh generation would be faster using GAMBIT. To have a complete series using FLUENT, the no fin and planar fin cases were also run with FLUENT.

A series of inviscid calculations were also made on the grid fin configuration. These simulations used the same geometry as the viscous calculations, except for the fin-body interface where a short circular stem was used for mesh generation purposes. A Cartesian flow solver, TIGER (Melton 1996, and Melton et al. 1995), and automatic Cartesian mesh generation program, CART3D (Aftosmis et al. 1998, and Aftosmis 1997), were used for the inviscid simulations. The Cartesian flow solver integrates the finite volume form of the Euler equations to steady state using a multistage Runge-Kutta time integration procedure (Melton 1996). The mesh generation and solution time were much less than the time required for the viscous

10

calculations. The Cartesian grid had about 1.3 M grid points, and the turnaround time was less than a day. The calculations for the flow solver were carried out on a Sun E10K machine on a single CPU. The flow solver took about 20 μs/cell/iteration and typically needed about 1500 iterations for convergence. The aerodynamic coefficients calculated with the inviscid simulations are compared to the viscous calculations in the following section.

The FLUENT simulations were performed in parallel using 4–6 processors on a Silicon Graphics (SGI) Onyx 2 with R12000 processors. The grid fin calculations took about 4.5 to 5 min/iteration using six processors. The aerodynamic coefficients converged in about 600 iterations. It took about 1,500 iterations for the turbulent viscosity to converge, with the scaled residual reduced to about 10^{-6}.

3. Results and Discussion

3.1   Aerodynamic Coefficients. Using the FLUENT postprocessor, the viscous and pressure forces were integrated along the missile body and fin surfaces to calculate the aerodynamic coefficients. The normal force (C_z), axial force (C_x), and pitching moment (C_m) coefficients are presented in missile-based coordinates, as shown in Figure 9. The pitching moment is expressed about the nose of the missile. The reference area is the cross-sectional area of the missile base, and the reference length is the diameter of the missile (94 mm). The calculated coefficients are compared to wind tunnel measurements performed at DERA (Simpson 1997). The DERA wind tunnel data did not include the forces on the base of the missile in the coefficient calculation. This value, which includes only the forebody and fin surfaces, is appropriate to compare to CFD calculations that do not include the base flow. The repeatability of the DERA data was reported to be within 1% at 2.5 Mach over the range of α investigated (Simpson 1997).

3.1.1 Body Alone Case (B1A). The aerodynamic coefficients calculated from the FLUENT and ZNSFLOW solutions are shown in Figures 10–12 and Table 1. Data from DERA wind
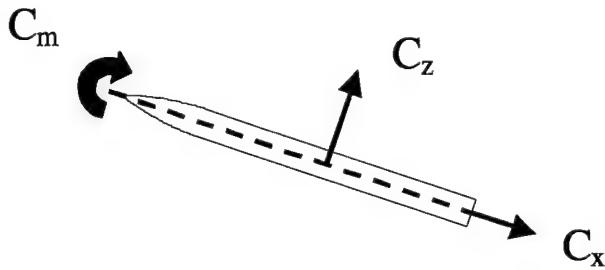
Figure 9. Axes and Sign Convention for Force and Moment Coefficients.

tunnel measurements are also shown. The calculated pitching moment coefficient (Figure 10), normal force coefficient (Figure 11), and axial force coefficient (Figure 12) are shown at $\alpha = 0°$, 10°, 14°, and 20° for the FLUENT calculations and at 0°, 4°, 10°, 14°, and 20° for the ZNSFLOW calculations. The calculated results show very good agreement with the measured aerodynamic coefficients. The maximum difference between the calculated and measured pitching moment coefficient was 3.6%, with the maximum occurring at $\alpha = 14°$ for the FLUENT calculations; it was 18%, with a maximum at $\alpha = 10°$ for the ZNSFLOW calculations. The maximum difference between the calculated and measured normal force coefficient was 2.0%, with the maximum occurring at $\alpha = 10°$ for the FLUENT calculations; it was 10%, with a maximum at $\alpha = 10°$ for the ZNSFLOW calculations. The maximum difference between the calculated and measured axial force coefficient was 4.2%, with the maximum occurring at $\alpha = 20°$ for the FLUENT calculations; it was 12%, with a maximum at $\alpha = 20°$ for the ZNSFLOW calculations. The difference calculation was not made at $\alpha = 0°$ for C_m and C_z, since these parameters are close to zero at this angle of attack.

3.1.2 Planar Fin Case (B1AC2R). The aerodynamic coefficients calculated from the FLUENT and ZNSFLOW solutions are also shown in Figures 10–12 and Table 1. The calculated coefficients are shown at $\alpha = 0°$, 10°, and 20° for the FLUENT calculations and at 0°, 4°, 10°, 14°, and 20° for the ZNSFLOW calculations. The calculated normal force and pitching
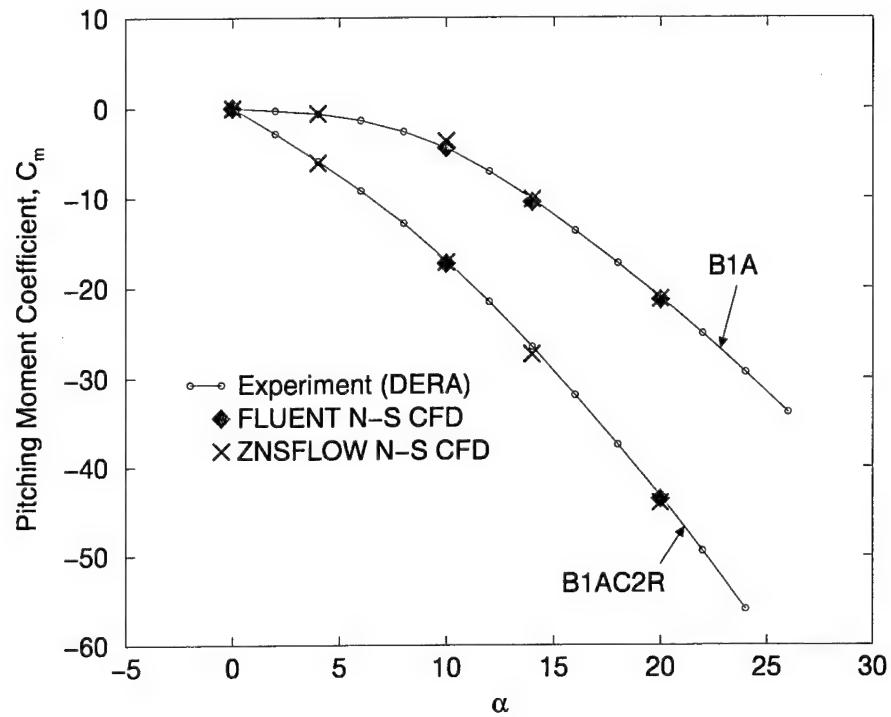
Figure 10. Pitching Moment Coefficient vs. α for B1A and B1AC2R Cases.
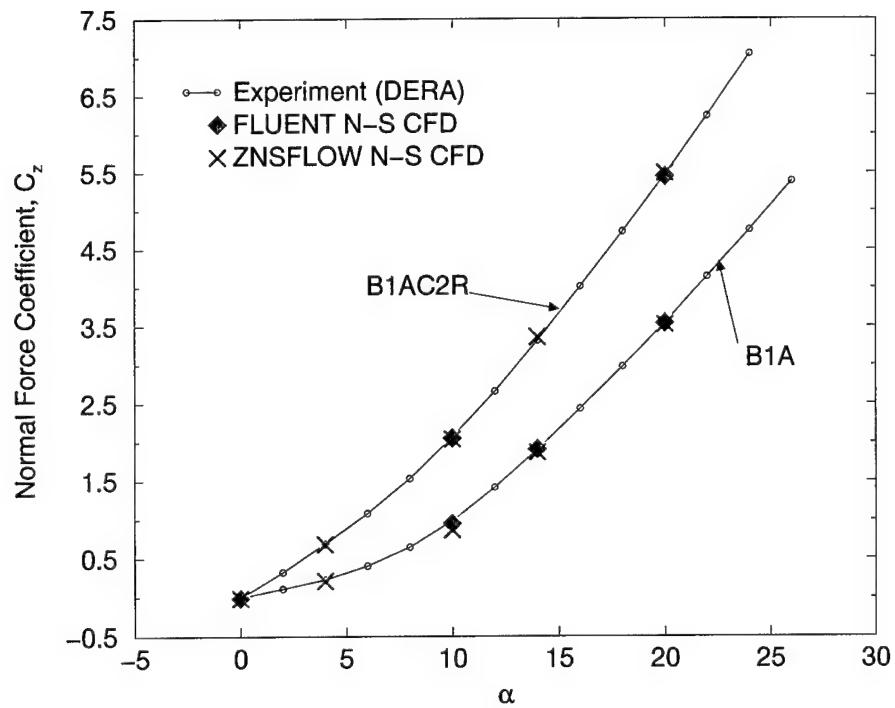
Figure 11. Normal Force Coefficient vs. α for B1A and B1AC2R Cases.

13
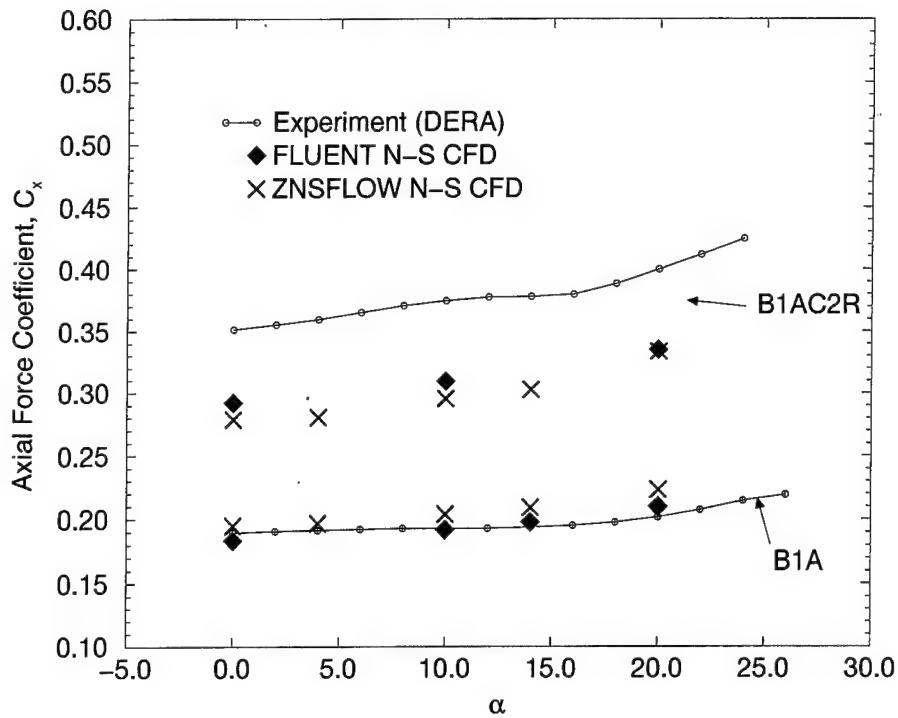
Figure 12. Axial Force Coefficient vs. α for B1A and B1AC2R Cases.

Table 1. Aerodynamic Coefficients vs. α (Mach No. 2.5, Reynolds No. 1.2 x 10⁶)

Case	α	C_m			C_n			C_x		
	(°)	Fluent	Exp.	%	Fluent	Exp.	%	Fluent	Exp.	%
B1A	0	0.000	−0.031	—	0.000	0.005	—	0.1837	0.1895	−3.1
	10	−4.445	−4.448	+0.1	0.961	0.981	−2.0	0.1919	0.1928	−0.5
	14	−10.49	−10.13	−3.6	1.919	1.897	+1.2	0.1977	0.1936	+2.1
	20	−21.36	−21.07	−1.4	3.548	3.543	+0.1	0.2098	0.2014	+4.2
B1AC2R	0	−0.004	0.041	—	0.000	−0.002	—	0.2922	0.3513	−16.8
	10	−17.27	−16.97	−1.8	2.060	2.065	−0.2	0.3095	0.3746	−17.4
	20	−43.61	−43.31	−0.7	5.454	5.465	−0.2	0.3349	0.3996	−16.2
B1AL2R	0	0.021	0.633	—	−0.002	0.081	—	0.5234	0.4677	+11.8
	10	−15.96	−17.01	+6.2	1.958	2.097	−6.6	0.5152	0.4859	+6.0
	12	−19.82	−21.07	+5.9	2.503	2.650	−5.5	0.5092	0.4807	+5.9
	20	−39.28	−40.43	+2.8	5.089	5.237	−2.8	0.4853	0.4711	+3.0

moment coefficients again show very good agreement with the measured aerodynamic coefficients. The maximum difference between the calculated and measured pitching moment coefficient was 1.8%, with the maximum occurring at $\alpha = 10°$ for the FLUENT calculations; it was 3.1%, with a maximum at $\alpha = 14°$ for the ZNSFLOW calculations. The maximum difference between the calculated and measured normal force coefficient was 0.2%, with the maximum occurring at $\alpha = 10°$ for the FLUENT calculations; it was 1.5%, with a maximum at $\alpha = 14°$ for the ZNSFLOW calculations.

The calculated axial force coefficients were lower than the measured values, but they predicted the same increase with α that the experimental data showed. The FLUENT calculations were within 17% of the experimental data, and the ZNSFLOW calculations were within 17–22%. The FLUENT calculations were probably closer to the experimental data because the one-equation turbulence model was used instead of the algebraic model used in ZNSFLOW. In addition, the thin-layer option used in the ZNSFLOW calculations eliminated the cross-stream turbulence effects in the fin region. Interestingly, in this case the predicted values of axial force are lower than the measured values. The opposite was found for the body alone case and the grid fin case. Some further investigation is warranted, and performing CFD calculations of the planar fin model, including part of the wind tunnel sting, has been proposed. Then, the CFD predictions can be directly compared to the main balance force measured in the wind tunnel to eliminate the experimental base pressure correction as the cause for the discrepancy. The viscous component of the axial force was about 40% of the total (regardless of angle of attack) in the FLUENT and ZNSFLOW simulations.

3.1.3 Grid Fin Case (B1AL2R).
The aerodynamic coefficients calculated from the FLUENT and the inviscid CART3D/TIGER solutions are shown in Figures 13–15 and Table 1. The calculated coefficients are shown at $\alpha = 0°$, $10°$, $12°$, and $20°$ for both CFD cases. The calculated normal force and pitching moment coefficients again show very good agreement with the measured aerodynamic coefficients. The maximum difference between the calculated and measured pitching moment coefficient was 6.2%, with the maximum occurring at $\alpha = 10°$ for the

15
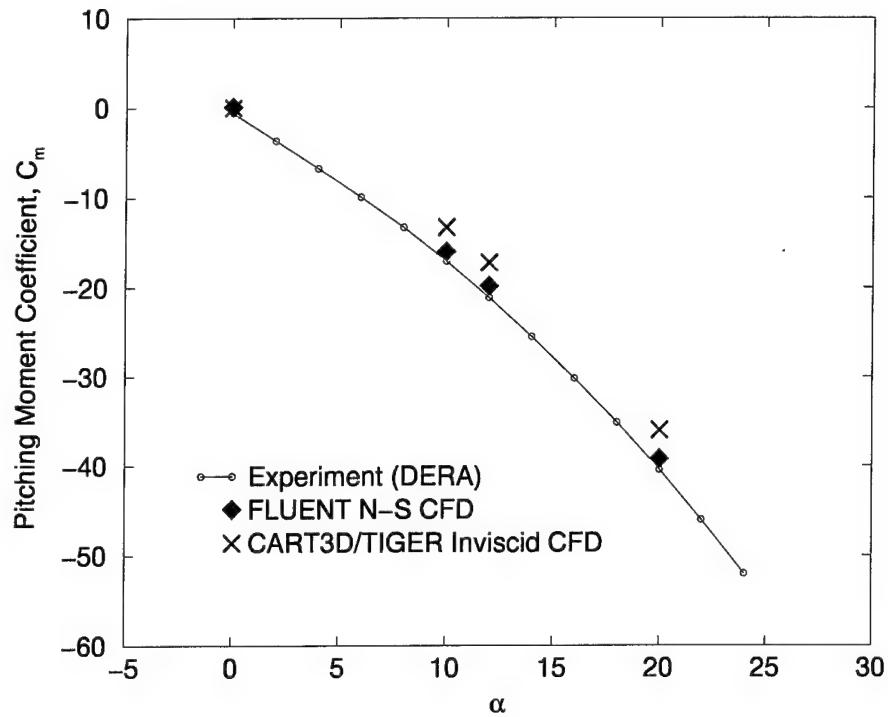
Figure 13. Pitching Moment Coefficient vs. α for B1AL2R Case.
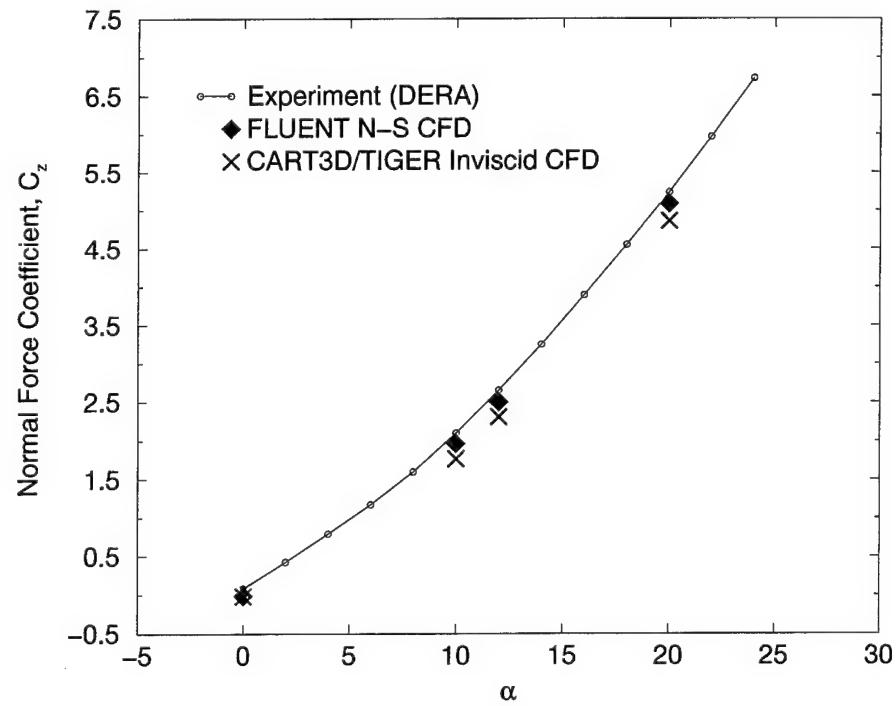
Figure 14. Normal Force Coefficient vs. α for B1AL2R Case.
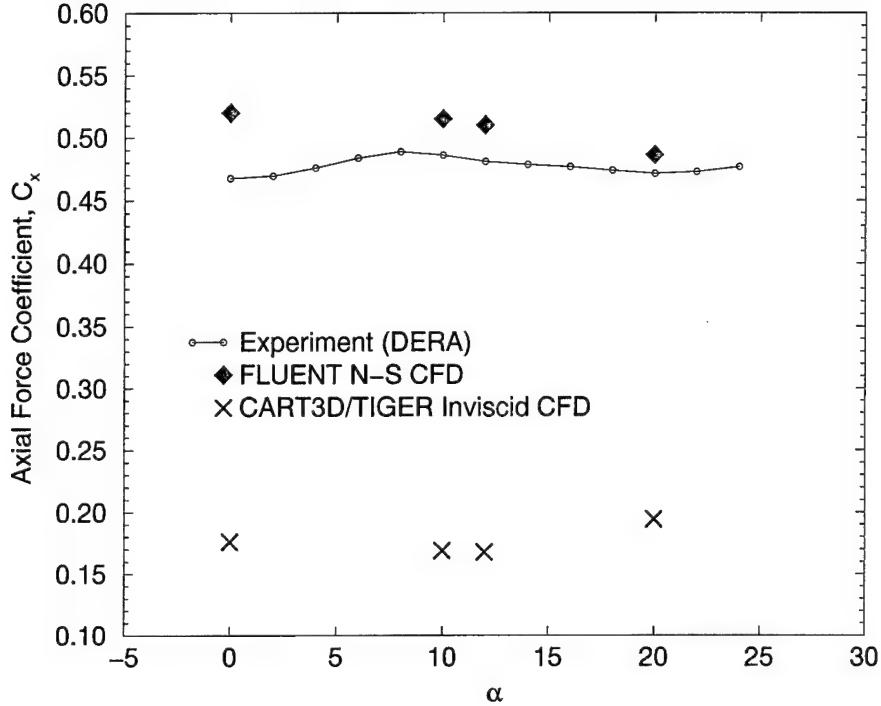
Figure 15. Axial Force Coefficient vs. α for B1AL2R Case.

FLUENT calculations; it was 18%, with a maximum at $\alpha = 12°$ for the CART3D/TIGER calculations. The maximum difference between the calculated and measured normal force coefficient was 6.6%, with the maximum occurring at $\alpha = 10°$ for the FLUENT calculations; it was 13%, with a maximum at $\alpha = 12°$ for the CART3D/TIGER calculations.

The FLUENT axial force calculations were a little higher than the measured values—a 3–6% difference for $\alpha > 0°$ and an 11% difference at $\alpha = 0°$. The inviscid CART3D/TIGER calculations underpredicted the axial force due to the absence of skin friction. However, the difference (about 60%) was larger than expected. If the viscous component is removed from the axial force coefficient calculated in the FLUENT simulations, the value is between 0.34 and 0.38; the axial force coefficients from the inviscid calculations are about one-half that (0.17–0.18). Some further investigation of this discrepancy is warranted, since other calculations of missiles in supersonic flow have resulted in more accurate results (Aftosmis 2000). Regardless of the angle of attack, the viscous component of the axial force was 29% of the total in the FLUENT simulations.

17

The inviscid calculations show that the total normal force and pitching moment data can be predicted to within 18% of the experimental data. If accurate axial force or drag information is not required, then the inviscid calculations may provide the information needed to check out multiple design approaches. Whether using CART3D/TIGER or an inviscid solution with FLUENT, the reduction in computing time is substantial.

3.1.4 Forces on Fins. The normal force coefficients on the individual grid fins from the FLUENT calculations are shown in Figure 16, along with the measured wind tunnel data (Simpson 1997) as a function of α. The fins are numbered 1–4, with fin 1 in the 3 o'clock position and fin 4 in the 12 o'clock position if looking forward from the rear of the missile in the "+" configuration. In the simulations, fins 1 and 3 are the same due to symmetry. The normal force on the fins was predicted very well, with the largest difference at about 11%. As expected, the normal force is greatest on the horizontal fins. The windward fin (fin 2, bottom) also provides a substantial normal force. The leeward fin (fin 4, top) provides a similar normal force as fin 2 up to about a 4° angle of attack, but then goes nonlinear and negative at higher angles of attack. As described by Simpson (1997), the nonlinear shape of the normal force vs. α curve for the leeward fin is caused by its location in the separated flow region at higher angles of attack. As shown later in plots of the flow field, the local angle of attack varies over the leeward grid fin. Some parts of the fin will be at an effective negative angle of attack, while other parts are at an effective positive angle of attack.

The axial force coefficients on individual grid fins were about 2–3 times greater than those on the planar fins. The viscous component of the axial force on the grid fin was about 1.5 times greater than on the planar fin. These values are presented in Table 2. Although it was speculated that the smaller chord of the grid fin might impart fewer viscous effects than a planar fin (Sun and Khalid 1998), the summation of the viscous effects of all the lattice surfaces of the grid fin leads to higher viscous forces. The likely reason inviscid calculations of the aerodynamic coefficients on a missile with grid fins were more accurate than those for a missile with planar fins (Sun and Khalid 1998) is that the viscous component, as a percentage of the total

18
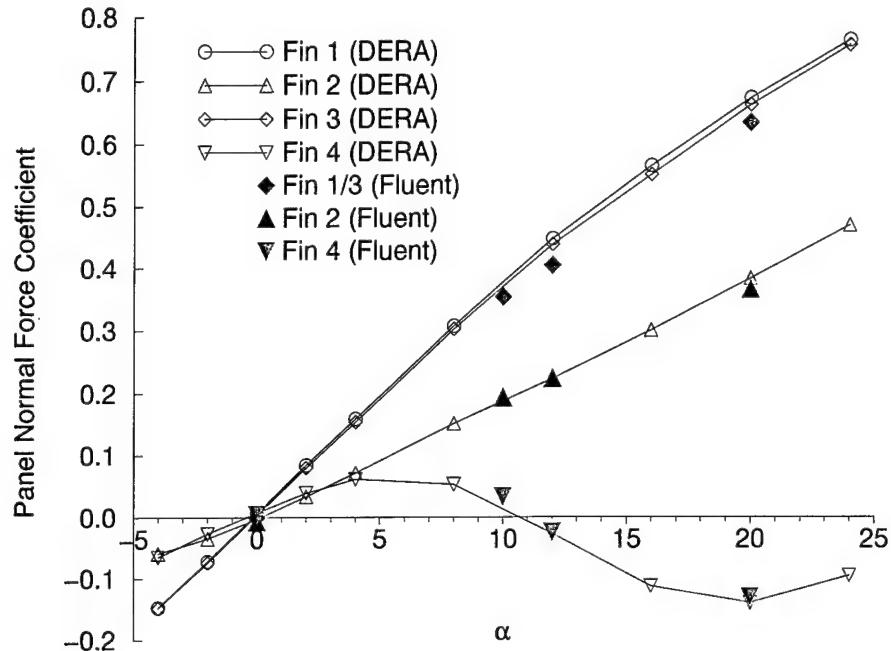
Figure 16. Normal Force Coefficient on Individual Grid Fins vs. α.

Table 2. Axial Force Coefficient on Fins (B1AC2R and B1AL2R Cases)

Planar Fin Case (B1AC2R)					Grid Fin Case (B1AL2R)				
α (°)	Fin	C_x Total (–)	C_x viscous (–)	% viscous (%)	α (°)	Fin	C_x total (–)	C_x viscous (–)	% viscous (%)
0	1/3	0.029	0.008	28	0	1/3	0.086	0.014	16
	2	0.029	0.008	28		2	0.085	0.014	16
	4	0.029	0.008	28		4	0.085	0.014	16
10	1/3	0.032	0.009	28	10	1/3	0.077	0.012	16
	2	0.032	0.010	31		2	0.091	0.014	15
	4	0.030	0.009	30		4	0.077	0.013	17
20	1/3	0.037	0.006	16	20	1/3	0.063	0.009	14
	2	0.042	0.012	29		2	0.104	0.016	15
	4	0.018	0.006	33		4	0.042	0.009	21

19

axial force on the fin, is less for the grid fin case. In this study, the viscous component of the axial force on the individual grid fin was about 16% of the total vs. about 30% for the planar fin. With a larger component of the axial force in the grid fin case due to form and wave drag, an inviscid calculation may be expected to compare better with measured data than a planar fin case.

3.2 Grid Fin Flow Field. Contour plots of Mach number on the symmetry plane are shown for the 10° and 20° angle of attack cases in Figures 17 and 18, respectively. A strong oblique shock is seen emanating from the windward side of the nose, with a weaker shock coming off of the leeward side. An expansion fan is seen coming off of the ogive-body interface. A large separated-flow region is seen coming off of the leeward side of the missile at $\alpha = 20°$, enclosing the top grid fin. The separation zone is smaller at $\alpha = 10°$.

3.26e+00
2.99e+00
2.72e+00
2.44e+00
2.17e+00
1.90e+00
1.63e+00
1.36e+00
1.09e+00
8.15e-01
5.43e-01
2.72e-01
0.00e+00
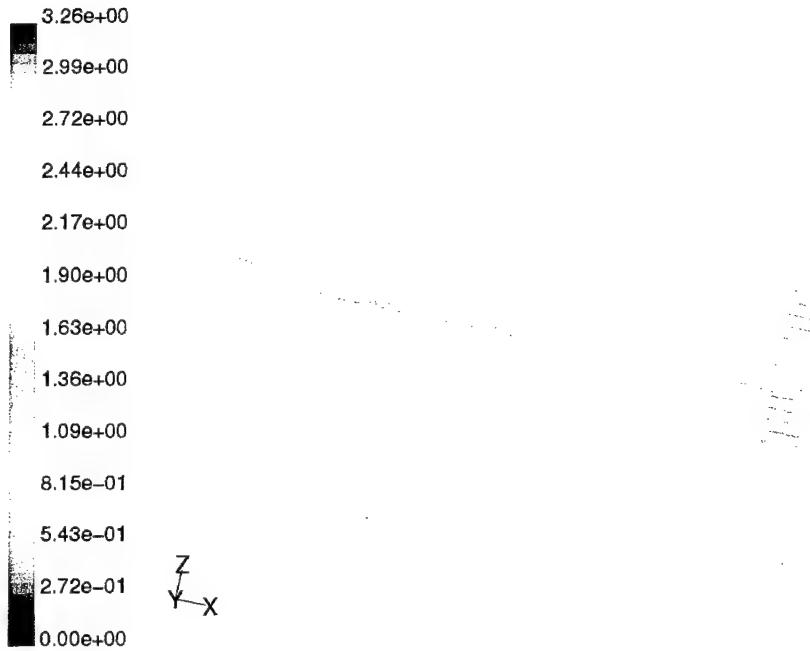
Figure 17. Mach Contours on Symmetry Plane for Grid Fin Case, $\alpha = 10°$.

4.00e+00
3.67e+00
3.33e+00
3.00e+00
2.67e+00
2.33e+00
2.00e+00
1.67e+00
1.33e+00
1.00e+00
6.67e-01
3.33e-01
0.00e+00
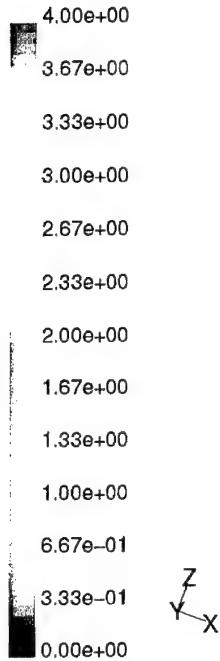
Figure 18. Mach Contours on Symmetry Plane for Grid Fin Case, $\alpha = 20°$.

There is a complex, three-dimensional shock structure emanating off of the grid fins. Figures 19 and 20 show pressure contours on the symmetry plane through the bottom and top fins, respectively, at $\alpha = 12°$. The outline of the grid fin frame is shown in the figures, with the shocks emanating off of the intersection of several grid fin cells (see Figures 7 and 8). At this Mach number, the shock and expansion waves do not reflect off of the interior walls of the grid fin cells (Washington and Miller 1998). Instead, they first reflect off of one another inside the grid fin cell, setting up several more reflections in the wake of the fin. In Figures 21 and 22, contours of Mach number are shown on the bottom and top fins for $\alpha = 12°$. For the bottom fin (Figure 21), the entire fin is at a positive relative angle of attack so that there is an expansion fan emanating from the lower part of each cell and a shock wave emanating off of the upper part of each cell. Part of the top fin (Figure 22) is at a negative relative angle of attack with respect to the incident flow; this is due to the vortices in the separation zone on the leeward side of the missile. The top cell is at a positive angle of attack, with the shock wave emanating from the top of the cell. The cell second from the top is nearly at a 0° angle of attack, with shock waves

21
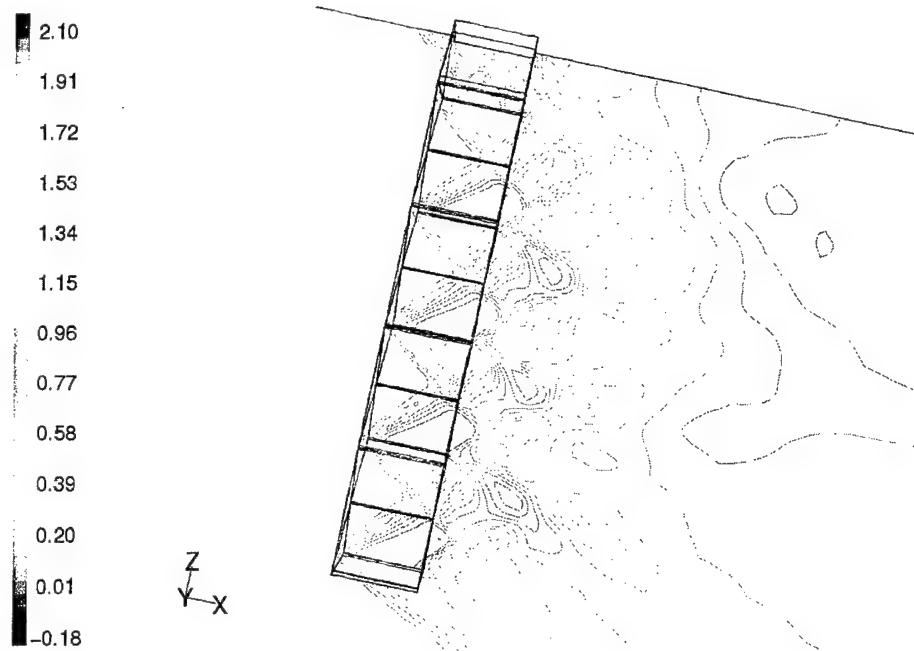
Figure 19. Pressure Coefficient Contours on Symmetry Plane Through Bottom Fin (Fin 2).
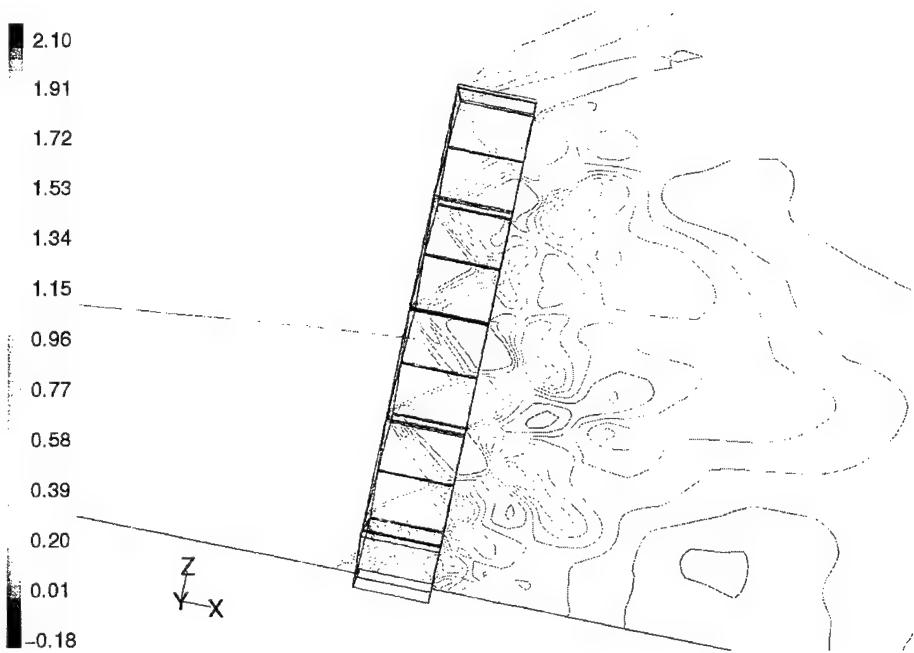
**Figure 20. Pressure Coefficient Contours on Symmetry Plane Through Top Fin (Fin 4).**

22
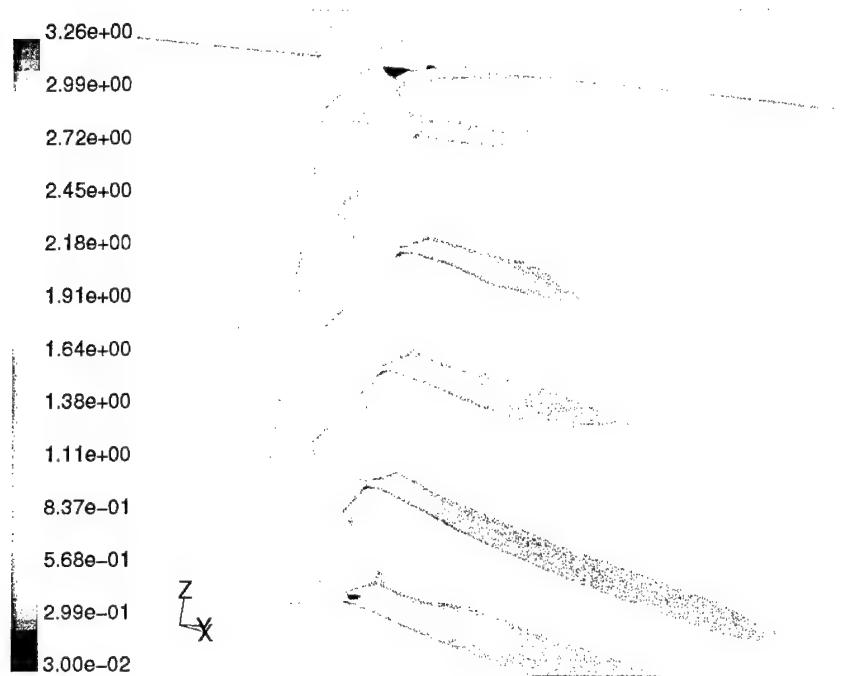
Figure 21. Mach Contours on Symmetry Plane Through Bottom Fin (Fin 2) at $\alpha = 12°$.
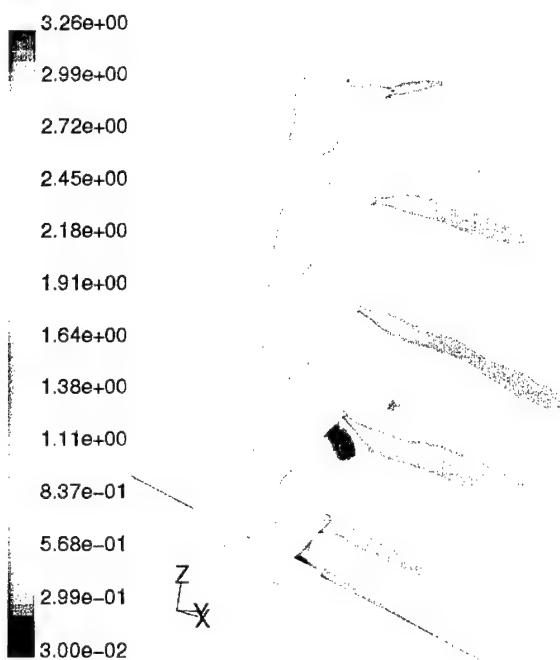
Figure 22. Mach Contours on Symmetry Plane Through Top Fin (Fin 4) at $\alpha = 12°$.

emanating from the top and bottom of the cell. The third and fourth cells from the top are at an effective negative angle of attack, with the shock wave emanating from the bottom of the cell. At $\alpha = 20°$ (Figures 23 and 24), the entire top fin was at a negative relative angle of attack. This flow structure is responsible for the negative normal forces observed on the top fin in wind tunnel tests and in these calculations (see Figure 16).

3.98e+00
3.65e+00
3.32e+00
2.99e+00
2.66e+00
2.33e+00
2.00e+00
1.67e+00
1.34e+00
1.02e+00
6.85e-01
3.56e-01
2.57e-02
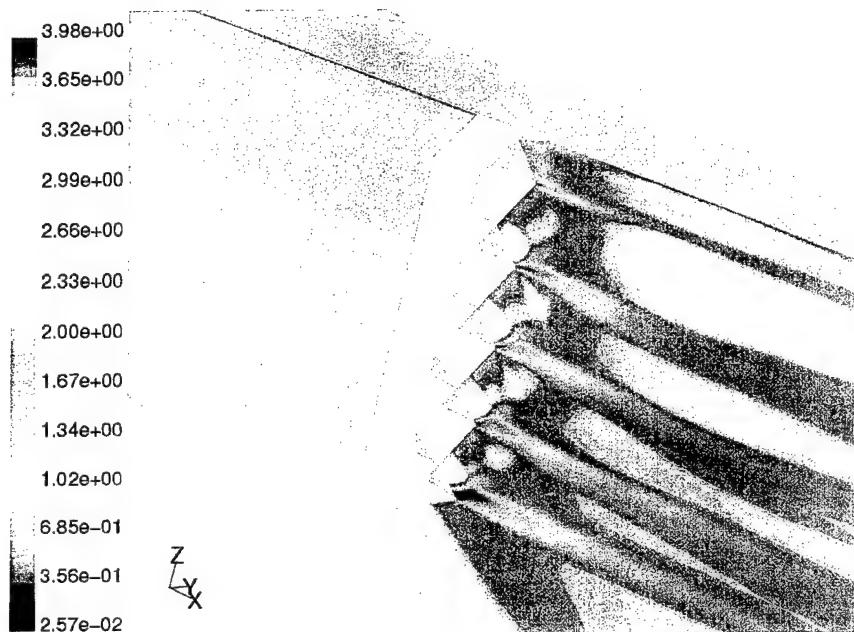
Figure 23. Mach Contours on Symmetry Plane Through Bottom Fin (Fin 2) at $\alpha = 20°$.

Contours of turbulent viscosity in the fin region are shown in Figures 25 and 26 for $\alpha = 10°$ and $\alpha = 20°$, respectively. The turbulent wakes downstream from each grid fin vane are evident in the figures. Note that the scale in Figure 26 is larger than the one in Figure 25. At $\alpha = 20°$, there is more interaction of the separated flow coming off of the missile body with the top grid fin.

4. Summary and Conclusions

Calculations of the viscous flow past a missile with grid fins were made using CFD simulations. The calculations were made at a Mach number of 2.5 and several angles of attack.
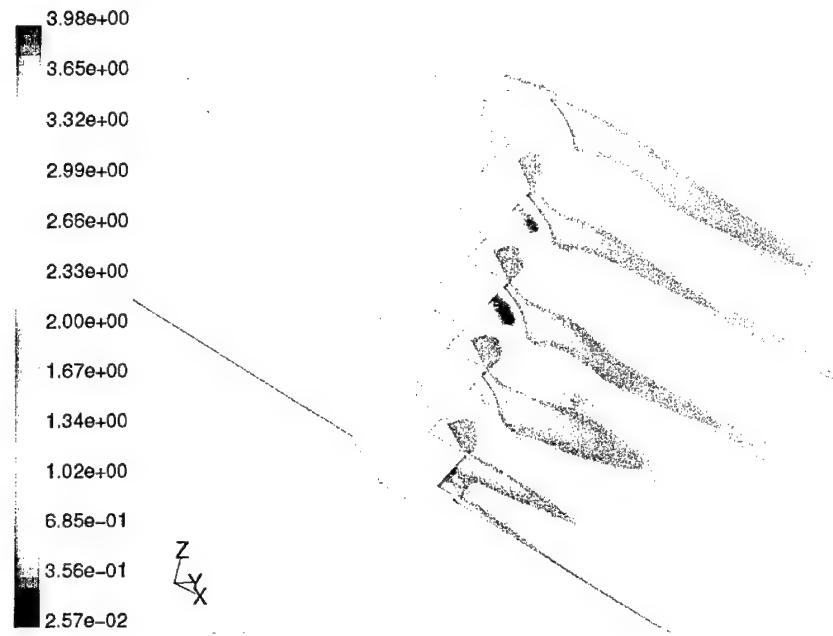
Figure 24. Mach Contours on Symmetry Plane Through Top Fin (Fin 4) at $\alpha = 20°$.
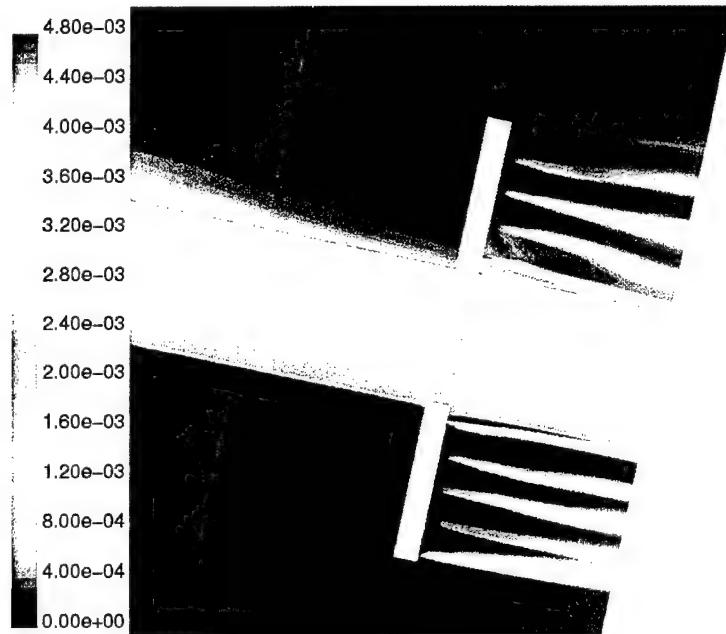
Figure 25. Turbulent Viscosity Contours on Symmetry Plane of Fin Region at $\alpha = 10°$.

1.50e-02	
1.37e-02	
1.25e-02	
1.12e-02	
9.98e-03	
8.74e-03	
7.49e-03	
6.24e-03	
4.99e-03	
3.74e-03	
2.50e-03	
1.25e-03	
0.00e+00	
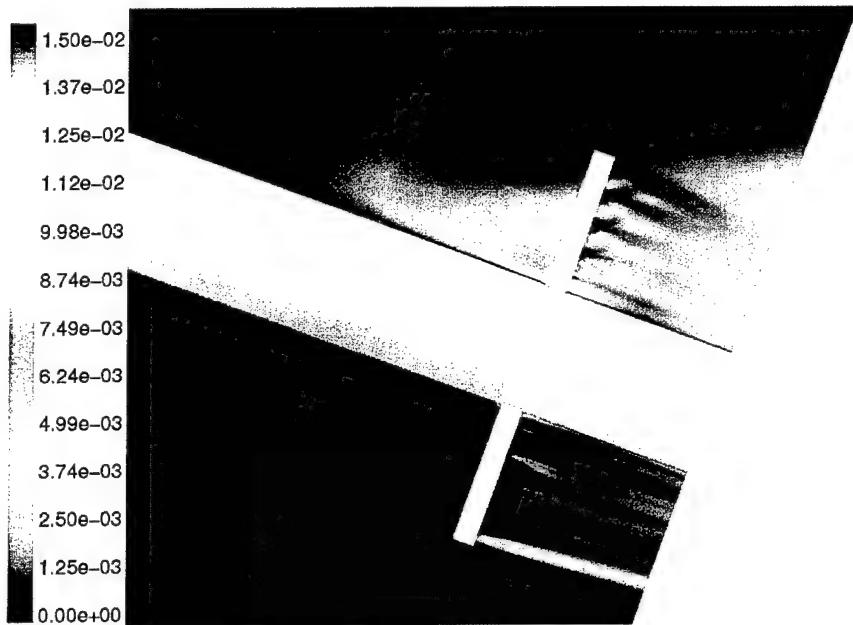
Figure 26. Turbulent Viscosity Contours on Symmetry Plane of Fin Region at $\alpha = 20°$.

The results were validated by comparing the computed aerodynamic coefficients for the missile and individual grid fins against detailed wind tunnel measurement data. The validation process also included calculating the flow field for the missile body alone and with conventional planar fins and comparing the calculations against wind tunnel data.

Very good agreement with the measured data was observed for all configurations investigated. For the grid fin case, the aerodynamic coefficients were within 6.6% of the wind tunnel data. The normal force coefficients on the individual grid fins were within 11% of the test data. The simulations were also successful in calculating the flow structure around the fin in the separated-flow region at the higher angles of attack. This was evident in the successful calculation of the nonlinear behavior for that fin, which showed negative normal force at the higher angles of attack. The physical nature of this effect was illustrated by presenting contours of Mach number on the symmetry plane through the vertical grid fins. The effective angle of attack is negative on part of or all of the top grid fin for the higher angles of attack.

26

The viscous component of the axial force on the grid fin was about 1.5 times greater than that on the planar fin. This contrasts previous speculation that the smaller chord of the grid fin would result in less viscous force than a planar fin. The total axial force on grid fin was about 2–3 times greater than that on the planar fin. As a percentage of the total force, the viscous component was about 16% for the grid fin and about 30% for the planar fin.

Results for inviscid calculations of the grid fin case were also presented. The normal force and pitching moment coefficients were calculated to within 18% of the experimental data. If axial force or drag information is not required, then inviscid calculations may provide reasonable design data in less time than viscous calculations.

The investigation detailed in this report demonstrated an approach for using viscous CFD simulations to calculate the flow field and aerodynamic coefficients for a missile with grid fins. Nevertheless, even when an unstructured mesh and wall functions were used to reduce the mesh size and computational requirements, substantial computing resources were required. An alternative approach would be to use the chimera overset grid technique to generate a structured mesh; however, the nature of the grid fin design makes the required resources large, regardless of the approach used. Inviscid calculations showed that the normal force and pitching moment coefficients could be calculated with reasonable accuracy.

INTENTIONALLY LEFT BLANK.

5. References

Abate, G., R. P. Duckerschein, and W. Hathaway. "Subsonic/Transonic Free-Flight Tests of a Generic Missile with Grid Fins." AIAA Paper 2000-0937, January 2000.

Abate, G., R. P. Duckerschein, and G. Winchenbach. "Free-Flight Testing of Missiles with Grid Fins." *Proceedings of the 50th Aeroballistic Range Association Meeting*, Pleasanton, CA, November 1999.

Aftosmis, M. J., Personal communication. NASA Ames Research Center, Moffett Field, CA, January 2000.

Aftosmis, M. J., M. J. Berger, and J. E. Melton. "Robust and Efficient Cartesian Mesh Generation for Component-Based Geometry." *AIAA Journal*, vol. 36, no. 6, pp. 952–960, 1998.

Aftosmis, M. J. "Solution Adaptive Cartesian Grid Methods for Aerodynamic Flows with Complex Geometries." *Computational Fluid Dynamics VKI Lectures Series 1997-05*, von Karman Institute for Fluid Dynamics, Belgium, 1997.

Burkhalter, J. E. "Grid Fins for Missile Applications in Supersonic Flow." AIAA Paper 96-0194, January 1996.

Burkhalter, J. E., and H. M. Frank. "Grid Fin Aerodynamics for Missile Applications in Subsonic Flow." *J. Spacecraft and Rockets*, vol. 33, no. 1, pp. 38-44, 1996.

Burkhalter, J. E., R. J. Hartfield, and T. M. Leleux. "Nonlinear Aerodynamic Analysis of Grid Fin Configurations." *J. of Aircraft*, vol. 32, no. 3, pp. 547-554, 1995.

Chen, S., M. Khalid, H. Xu, and F. Lesage. "A Comprehensive CFD Investigation of Grid Fins as Efficient Control Surface Devices." AIAA Paper 2000-0987, January 2000.

Edge, H. L., J. Sahu, W. B. Sturek, D. M. Pressel, K. R. Heavey, P. Weinacht, C. K. Zoltani, C. J. Nietubicz, J. Clarke, M. Behr, and P. Collins. "Common High Performance Computing Software Support Initiative (CHSSI) Computational Fluid Dynamics (CFD)-6 Project Final Report: ARL Block-Structured Gridding Zonal Navier-Stokes Flow (ZNSFLOW) Solver Software." U. S. Army Research Laboratory, ARL-TR-2084, Aberdeen Proving Ground, MD, February 2000.

Fluent 5.0 Users Guide, Vol. 2. Lebanon, NH: Fluent, Inc., 1998.

Khalid, M., Y. Sun, and H. Xu. "Computation of Flows Past Grid Fin Missiles." *Proceedings of the NATO RTO-MP-5, Missile Aerodynamics*, NATO Research and Technology Organization, November 1998.

Kretzschmar, R. W., and J. E. Burkhalter. "Aerodynamic Prediction Methodology for Grid Fins." *Proceedings of the NATO RTO-MP-5, Missile Aerodynamics*, NATO Research and Technology Organization, November 1998.

Lesage, F. "Numerical Investigation of the Supersonic Flow Inside a Grid Fin Cell." *Proceedings of the 17th International Symposium on Ballistics*, vol. 1, American Defense Preparedness Association, Arlington, VA, pp. 209–216, 1998.

Melton, J. E. "Automated Three-Dimensional Cartesian Grid Generation and Euler Flow Solutions for Arbitrary Geometries." Ph.D. dissertation, University of California Davis, June 1996.

Melton, J. E., M. J. Berger, M. J. Aftosmis, and M. D. Wong. "3-D Applications of a Cartesian Grid Euler Method." AIAA Paper 95-0853, January 1995.

Miller, M. S., and W. D. Washington. "An Experimental Investigation of Grid Fin Drag Reduction Techniques." AIAA Paper 94-1914-CP, June 1994.

Simpson, G. M., and A. J. Sadler. "Lattice Controls: A Comparison with Conventional, Planar Fins." *Proceedings of the NATO RTO-MP-5, Missile Aerodynamics*, NATO Research and Technology Organization, November 1998.

Simpson, G. "A Preliminary Analysis of the DERA Lattice Controls Database." Defense Research Agency, DERA/AS/HWA/WP97196/1.0, Farnborough, UK, July 1997.

Spalart, P. R., and S. R. Allmaras. "A One-Equation Turbulence Model for Aerodynamic Flows." AIAA Paper 92-0439, January 1992.

Steger, J. L., F. C. Dougherty, and J. A. Benek. "A Chimera Grid Scheme." *Advances in Grid Generation*, edited by K. N. Ghia and U. Ghia, American Society of Mechanical Engineers, ASME FED-5, New York, June 1983.

Sun, Y., and M. Khalid. "A CFD Investigation of Grid Fin Missiles." AIAA Paper 98-3571, July 1998.

Tong, Z., Z. Lu, and X. Shen. "Calculation and Analysis of Grid Fin Configurations." *Advances in Astronautical Sciences*, AAS 95-647, 1996.

Washington, W. D., and M. S. Miller. "Experimental Investigations of Grid Fin Aerodynamics: A Synopsis of Nine Wind Tunnel and Three Flight Tests." *Proceedings of the NATO RTO-MP-5, Missile Aerodynamics*, NATO Research and Technology Organization, November 1998.

Washington, W. D., and M. S. Miller. "Grid Fins – A New Concept for Missile Stability and Control." AIAA Paper 93-0035, January 1993.

INTENTIONALLY LEFT BLANK.

NO. OF COPIES	ORGANIZATION	NO. OF COPIES	ORGANIZATION
2	DEFENSE TECHNICAL INFORMATION CENTER DTIC DDA 8725 JOHN J KINGMAN RD STE 0944 FT BELVOIR VA 22060-6218	1	DIRECTOR US ARMY RESEARCH LAB AMSRL D D R SMITH 2800 POWDER MILL RD ADELPHI MD 20783-1197
1	HQDA DAMO FDT 400 ARMY PENTAGON WASHINGTON DC 20310-0460	1	DIRECTOR US ARMY RESEARCH LAB AMSRL DD 2800 POWDER MILL RD ADELPHI MD 20783-1197
1	OSD OUSD(A&T)/ODDDR&E(R) R J TREW THE PENTAGON WASHINGTON DC 20301-7100	1	DIRECTOR US ARMY RESEARCH LAB AMSRL CI AI R (RECORDS MGMT) 2800 POWDER MILL RD ADELPHI MD 20783-1145
1	DPTY CG FOR RDA US ARMY MATERIEL CMD AMCRDA 5001 EISENHOWER AVE ALEXANDRIA VA 22333-0001	3	DIRECTOR US ARMY RESEARCH LAB AMSRL CI LL 2800 POWDER MILL RD ADELPHI MD 20783-1145
1	INST FOR ADVNCD TCHNLGY THE UNIV OF TEXAS AT AUSTIN PO BOX 202797 AUSTIN TX 78720-2797	1	DIRECTOR US ARMY RESEARCH LAB AMSRL CI AP 2800 POWDER MILL RD ADELPHI MD 20783-1197
1	DARPA B KASPAR 3701 N FAIRFAX DR ARLINGTON VA 22203-1714		ABERDEEN PROVING GROUND
1	NAVAL SURFACE WARFARE CTR CODE B07 J PENNELLA 17320 DAHLGREN RD BLDG 1470 RM 1101 DAHLGREN VA 22448-5100	4	DIR USARL AMSRL CI LP (BLDG 305)
1	US MILITARY ACADEMY MATH SCI CTR OF EXCELLENCE MADN MATH MAJ HUBER THAYER HALL WEST POINT NY 10996-1786		

NO. OF COPIES	ORGANIZATION	NO. OF COPIES	ORGANIZATION
7	CDR US ARMY ARDEC AMSTE AET A R DEKLEINE C NG R BOTTICELLI H HUDGINS J GRAU S KAHN W KOENIG PICATINNY ARSENAL NJ 07806-5001	1	NAVAL AIR WARFARE CENTER D FINDLAY MS 3 BLDG 2187 PATUXENT RIVER MD 20670
1	CDR US ARMY ARDEC AMSTE CCH V P VALENTI PICATINNY ARSENAL NJ 07806-5001	1	DEFENSE INTELLIGENCE AGENCY MISSILE AND SPACE INT. CENTER MSA-1 A NICHOLSON BLDG 4545 FOWLER ROAD REDSTONE ARSENAL AL 35898-5500
1	CDR US ARMY ARDEC SFAE FAS SD M DEVINE PICATINNY ARSENAL NJ 07806-5001	4	DIR NASA LANGLEY RESEARCH CENTER TECH LIBRARY D M BUSHNELL DR M J HEMSCH DR J SOUTH LANGLEY STATION HAMPTON VA 23665
2	USAF WRIGHT AERONAUTICAL LABS AFWAL FIMG DR J SHANG N E SCAGGS WPAFB OH 45433-6553	2	DARPA DR P KEMMEY DR J RICHARDSON 3701 NORTH FAIRFAX DR ARLINGTON VA 22203-1714
3	AIR FORCE ARMAMENT LAB AFATL/FXA S C KORN B SIMPSON D BELK EGLIN AFB FL 32542-5434	8	DIR NASA AMES RESEARCH CENTER T 27B-1 L SCHIFF T 27B-1 T HOLST MS 237-2 D CHAUSSEE MS 269-1 M RAI MS 200-6 P KUTLER MS 258 1 B MEAKIN MS T27B-2 M AFTOSMIS MS T27B-2 J MELTON MOFFETT FIELD CA 94035
1	AFRL/MNAV G ABATE 101 W EGLIN BLVD, STE 219 EGLIN AFB FL 32542		
1	CDR NSWC CODE B40 DR W YANTA DAHLGREN VA 22448-5100	1	DIR NASA LANGLEY RESEARCH CENTER MS 499 P BUNING HAMPTON VA 23681
1	CDR NSWC CODE 420 DR A WARDLAW INDIAN HEAD MD 20640-5035	2	USMA DEPT OF MECHANICS LTC A L DULL M COSTELLO WEST POINT NY 10996
1	CDR NSWC DR F MOORE DAHLGREN VA 22448		

NO. OF COPIES	ORGANIZATION	NO. OF COPIES	ORGANIZATION
5	CDR USAAMCOM AMSAM RD SS AT E KREEGER G LANDINGHAM C D MIKKELSON E VAUGHN W D WASHINGTON REDSTONE ARSENAL AL 35898-5252	1	METACOMP TECHNOLOGIES INC S R CHAKRAVARTHY 650 HAMPSHIRE ROAD SUITE 200 WESTLAKE VILLAGE CA 91361-2510
1	COMMANDER US ARMY TACOM-ARDEC BLDG 162S AMCPM DS MO P J BURKE PICATINNY ARSENAL NJ 07806-5000	2	ROCKWELL SCIENCE CENTER S V RAMAKRISHNAN V V SHANKAR 1049 CAMINO DOS RIOS THOUSAND OAKS CA 91360
2	UNIV OF CALIFORNIA DAVIS DEPT OF MECHANICAL ENGRG H A DWYER M HAFEZ DAVIS CA 95616	1	ADVANCED TECHNOLOGY CTR ARVIN/CALSPAN AERODYNAMICS RESEARCH DEPT DR M S HOLDEN PO BOX 400 BUFFALO NY 14225
1	AEROJET ELECTRONICS PLANT D W PILLASCH B170 DEPT 5311 PO BOX 296 1100 WEST HOLLYVALE STREET AZUSA CA 91702	1	UNIV OF ILLINOIS AT URBANA CHAMPAIGN DEPT OF MECH AND IND ENGRG DR J C DUTTON URBANA IL 61801
1	MIT TECH LIBRARY 77 MASSACHUSETTS AVE CAMBRIDGE MA 02139	1	UNIVERSITY OF MARYLAND DEPT OF AEROSPACE ENGRG DR J D ANDERSON JR COLLEGE PARK MD 20742
1	GRUMANN AEROSPACE CORP AEROPHYSICS RESEARCH DEPT DR R E MELNIK BETHPAGE NY 11714	1	UNIVERSITY OF NOTRE DAME DEPT OF AERONAUTICAL AND MECH ENGINEERING T J MUELLER NOTRE DAME IN 46556
1	MICRO CRAFT INC DR J BENEK 207 BIG SPRINGS AVE TULLAHOMA TN 37388-0370	1	UNIVERSITY OF TEXAS DEPT OF AEROSPACE ENGRG MECH DR D S DOLLING AUSTIN TX 78712-1055
1	LANL B HOGAN MS G770 LOS ALAMOS NM 87545	1	UNIVERSITY OF DELAWARE DEPT OF MECH ENGINEERING DR J MEAKIN NEWARK DE 19716
		2	LOCKHEED MARTIN VOUGHT SYS PO BOX 65003 M/S EM 55 P WOODEN W B BROOKS DALLAS TX 75265-0003

NO. OF COPIES	ORGANIZATION
2	FLUENT INC G STUCKERT 10 CAVENDISH COURT CENTERRA RESOURCE PARK LEBANON NH 03766-1442

ABERDEEN PROVING GROUND

3	CDR US ARMY ARDEC FIRING TABLES BRANCH R LIESKE R EITMILLER F MIRABELLE BLDG 120

29	DIR USARL
	AMSRL CI
	  N RADHAKRISHNAN
	AMSRL CI H
	  C NIETUBICZ
	  D HISLEY
	  A MARK
	  W STUREK
	AMSRL CI LP
	  TECH LIBRARY (2 CPS)
	AMSRL WM
	  E SCHMIDT
	  T ROSENBERGER
	AMSRL WM B
	  A W HORST JR
	  W CIEPIELLA
	AMSRL WM BA
	  W D'AMICO
	  T BROWN
	  L BURKE
	  J CONDON
	  B DAVIS
	  M HOLLIS
	AMSRL WM BC
	  P PLOSTINS
	  M BUNDY
	  G COOPER
	  H EDGE
	  J GARNER
	  B GUIDOS
	  K HEAVEY
	  D LYON
	  A MIKHAIL
	  V OSKAY
	  J SAHU
	  K SOENCKSEN

NO. OF COPIES	ORGANIZATION
	ABERDEEN PROVING GROUND

14	DIR USARL
	AMSRL WM BC
	  D WEBB
	  P WEINACHT
	  S WILKERSON
	  A ZIELINSKI
	AMSRL WM BD
	  B FORCH
	AMSRL WM BE
	  G WREN
	  M NUSCA
	  J DESPIRITO (5 CPS)
	AMSRL WM BF
	  J LACETERA
	AMSRL WM TB
	  R LOTTERO

2   DEFENCE EVALUATION AND
RESEARCH AGENCY
A J SADLER
G SIMPSON
BEDFORD MK41 6AE
UNITED KINGDOM

3   DEF RESEARCH ESTABLISHMENT
VALCARTIER
F LESAGE
E FOURNIER
A DUPUIS
2459 PIE-XI BLVD NORTH
VAL-BELAIR (QC) G3J 1X5
CANADA

INTENTIONALLY LEFT BLANK.

REPORT DOCUMENTATION PAGE

1. AGENCY USE ONLY *(Leave blank)*	2. REPORT DATE	3. REPORT TYPE AND DATES COVERED
	September 2000	Final, Dec 98 - Oct 99

4. TITLE AND SUBTITLE
Computational Fluid Dynamic (CFD) Analysis of a Generic Missile With Grid Fins

5. FUNDING NUMBERS
PR: 1L162618AH80

6. AUTHOR(S)
James DeSpirito, Harris L. Edge, Paul Weinacht, Jubaraj Sahu, and Surya Dinavahi*

7. PERFORMING ORGANIZATION NAME(S) AND ADDRESS(ES)
U.S. Army Research Laboratory
ATTN: AMSRL-WM-BC
Aberdeen Proving Ground, MD 21005-5066

8. PERFORMING ORGANIZATION REPORT NUMBER
ARL-TR-2318

9. SPONSORING/MONITORING AGENCY NAMES(S) AND ADDRESS(ES)

10. SPONSORING/MONITORING AGENCY REPORT NUMBER

11. SUPPLEMENTARY NOTES
*Mississippi State University

12a. DISTRIBUTION/AVAILABILITY STATEMENT
Approved for public release; distribution is unlimited.

12b. DISTRIBUTION CODE

13. ABSTRACT *(Maximum 200 words)*

This report presents the results of a study demonstrating an approach for using viscous computational fluid dynamic simulations to calculate the flow field and aerodynamic coefficients for a missile with grid fins. A grid fin is an unconventional lifting and control surface that consists of an outer frame supporting an inner grid of intersecting planar surfaces of small chord. The calculations were made at a Mach number of 2.5 and several angles of attack for a missile without fins, with planar fins, and with grid fins. The results were validated by comparing the computed aerodynamic coefficients for the missile and individual grid fins against wind tunnel measurement data. Very good agreement with the measured data was observed for all configurations investigated. For the grid fin case, the aerodynamic coefficients were within 2.8–6.5% of the wind tunnel data. The normal force coefficients on the individual grid fins were within 11% of the test data. The simulations were also successful in calculating the flow structure around the fin in the separated-flow region at the higher angles of attack. This was evident in the successful calculation of the nonlinear behavior for that fin, which showed negative normal force at the higher angles of attack. The effective angle of attack is negative on either part of or all of the top grid fin for the higher angles of attack.

14. SUBJECT TERMS
grid fins, lattice controls, computational fluid dynamics, Navier-Stokes, missile aerodynamics

15. NUMBER OF PAGES
42

16. PRICE CODE

17. SECURITY CLASSIFICATION OF REPORT	18. SECURITY CLASSIFICATION OF THIS PAGE	19. SECURITY CLASSIFICATION OF ABSTRACT	20. LIMITATION OF ABSTRACT
UNCLASSIFIED	UNCLASSIFIED	UNCLASSIFIED	UL

INTENTIONALLY LEFT BLANK.

USER EVALUATION SHEET/CHANGE OF ADDRESS

This Laboratory undertakes a continuing effort to improve the quality of the reports it publishes. Your comments/answers to the items/questions below will aid us in our efforts.

1. ARL Report Number/Author___ARL-TR-2318 (Despirito)_____ Date of Report___September 2000_____

2. Date Report Received _____

3. Does this report satisfy a need? (Comment on purpose, related project, or other area of interest for which the report will be used.) _____

_____

_____

4. Specifically, how is the report being used? (Information source, design data, procedure, source of ideas, etc.) _____

_____

_____

5. Has the information in this report led to any quantitative savings as far as man-hours or dollars saved, operating costs avoided, or efficiencies achieved, etc? If so, please elaborate. _____

_____

_____

6. General Comments. What do you think should be changed to improve future reports? (Indicate changes to organization, technical content, format, etc.) _____

_____

_____

_____

_____
Organization

CURRENT
ADDRESS
_____
Name   E-mail Name
_____
Street or P.O. Box No.
_____
City, State, Zip Code

7. If indicating a Change of Address or Address Correction, please provide the Current or Correct address above and the Old or Incorrect address below.

_____
Organization

OLD
ADDRESS
_____
Name
_____
Street or P.O. Box No.
_____
City, State, Zip Code

(Remove this sheet, fold as indicated, tape closed, and mail.)
(DO NOT STAPLE)